On-State Voltage Measurement Circuit for Condition Monitoring of MOSFETs in Resonant Converters

electronics

MDPI

Article

On-State Voltage Measurement Circuit for Condition Monitoring of MOSFETs in Resonant Converters

Marco Ventimiglia [1], Alfio Scuto [1], Giuseppe Sorrentino [1], Gaetano Belverde [1], Francesco Iannuzzo [2] and Santi Agatino Rizzo [3,*]

[1] STMicroelectronics, 95121 Catania, Italy; marco.ventimiglia@st.com (M.V.); alfio.scuto@st.com (A.S.); giuseppe.sorrentino@st.com (G.S.); gaetano.belverde@st.com (G.B.)
[2] Department of Energy Technology, Aalborg University, 9220 Aalborg, Denmark; fia@energy.aau.dk
[3] Department of Electrical Electronic and Computer Engineering (DIEEI), University of Catania, 95125 Catania, Italy
* Correspondence: santi.rizzo@unict.it

Abstract: This work aims to estimate the Metal-Oxide-Semiconductor Field-Effect Transistor's (MOSFET) junction temperature, guessing in real time the dynamic drain-source resistance during MOSFET operation in LLC (Inductor-Inductor-Capacitor) converters usually adopted in Switched-Mode Power Supplies. The task is accomplished using an on-state voltage measurement circuit that allows clamping of the high-voltage drain-source voltage during the off-state. The results of this method have been compared with the temperature accurately measured using a co-packed die as a thermal sensor.

Keywords: power electronics; reliability; power MOSFET

Citation: Ventimiglia, M.; Scuto, A.; Sorrentino, G.; Belverde, G.; Iannuzzo, F.; Rizzo, S.A. On-State Voltage Measurement Circuit for Condition Monitoring of MOSFETs in Resonant Converters. *Electronics* **2024**, *13*, 3902. https://doi.org/10.3390/electronics13193902

Academic Editor: Fabio Corti

Received: 13 August 2024
Revised: 18 September 2024
Accepted: 24 September 2024
Published: 2 October 2024

1. Introduction

Power semiconductor devices are widely used in various applications to increase the efficiency of electrical/electronic systems and improve their control [1]. The increasing demand for highly efficient and simultaneously small-sized electronic systems has increased the use of improved packages [2], better devices [3], and resonant converters [4]. As the power density increases, power devices face more critical thermal issues, making on-line condition monitoring even more important. Therefore, considering that power semiconductor devices are key components in many electrical systems, their reliability has been studied extensively due to their vulnerability to the temperature fluctuations that occur during working operations [5].

Unfortunately, reliability prediction is, in general, very challenging in real applications, especially those where power electronics are subject to arbitrary mission profiles. Condition monitoring is a widely used approach to mitigate uncertainty in the predicted remaining useful life of power electronic converters. Among other benefits, condition-monitoring strategies allow the development of improved predictive maintenance plans [6]. It is worth mentioning that the adoption of condition monitoring circuits in real applications is limited by (1) cost, (2) intrusiveness, and (3) the reduction in the expected life that is introduced on the monitored converter due to the inevitable modifications [7].

In general, condition-monitoring strategies rely on inferring the junction temperature swing and maximum junction temperature from indirect measurements, such as voltages or delays. The reason for that is, according to established and widely recognized models adopted in the field, the number of cycles to failure is related through an inverse power law to the two aforementioned temperatures [8,9].

Some condition-monitoring methods are based on the on-state drain-source voltage (V_{DS}) and adopt the so-called On-state Voltage Measurement Circuits (OVMCs) to measure it [10,11]. $V_{DS,on}$ has been used for a long time as a temperature-sensitive electrical parameter (TSEP) to estimate the junction temperature either in Silicon MOSFET, SiC MOSFET,

or GaN MOSFET [12–16]. A simple circuit was developed in [12] to monitor, using a microcontroller, the health condition of a SiC MOSFET module in terms of bond-wire fatigue and metallization reconstruction. However, the temperature measurement is performed externally to the frame, and consequently, a large distance from the die negatively affects the accuracy. In fact, integration of the temperature sensor close to the die is difficult in the TO247-4 package. In detail, integrating this additional sensor becomes more complex due to the limited space and the limit on the number of available pins in comparison with a power module [17]. The characterization for condition monitoring of state-of-the-art 1.2 kV SiC MOSFETs from various semiconductor manufacturers was performed in [13]. In [14], an aging effect model and decoupling method have been presented and verified by experiments based on a thermal cycle-accelerated aging test. A circuit with an auxiliary MOSFET was proposed in [15] to measure the on-state voltage drop on-line. An on-line junction temperature measurement method based on the on-state resistance calculated using the on-state voltage and on-state current was discussed in [16]. However, these methods cannot be used for on-line condition monitoring but for characterization purposes only. More specifically, these methods adopt heaters or ovens to warm the devices to investigate the relationship between temperature and on-state voltage (or resistance). This approach prevents their use in on-line condition monitoring.

Remarkably, OVMCs are usually designed for low-side devices, while only a few works have addressed high-side OVMCs [18–21]. This implies that research focusing on on-line condition monitoring of high-side MOSFET is very limited. In detail, an on-line condition-monitoring approach has been proposed in [18] to estimate the on-resistance degradation in real time for the high-side switch. However, this approach is developed for a 12 V buck converter; thus, the design of an OVMC circuit is facilitated due to the low-voltage levels. Thus, further reducing the number of works adopting high-side OVMCs for high-voltage MOSFETs: (1) an in-situ current sensing circuit integrating the controller to improve operational capabilities while performing condition monitoring has been described in [19]; (2) in [20] an on-state voltage sensor that enables real-time monitoring has been presented; and (3) [21] presents the challenges of implementing in-situ prognostics to practical power converters and proposes a new on-state voltage monitoring circuit for the high-side power transistors. However, the adoption of a resistor in the diode biasing circuit causes a biasing current that varies according to the measured on-state voltage; consequently, the offset introduced by the circuit depends on the drain current and on-state resistance of the device.

In LLC converters, OVMC must also be used for dissipated power measurements; hence, the circuit must measure negative voltages to evaluate the power dissipated during the conduction of the body diode. The previous circuits [18–21] present isolated amplifiers that impede the measurement of negative voltages, preventing their use in resonant converters. To the authors' best knowledge, no study has been conducted so far, except for a recent and remarkable paper on a calorimetric method used to measure the power dissipated during MOSFET switching in a high-efficiency LLC resonant converter [22].

In conclusion, this paper presents an accurate on-line MOSFET junction temperature estimation method based on an OVMC that is suitable for resonant converters. The calibration and validation of the proposed method were performed using a laboratory prototype that embedded a co-packed die used as a reference sensor. The validation has been carried out for various LLC loads and, consequently, for a wide range of temperatures that also reach the device's maximum temperature. According to the previous considerations, the motivation, contribution, and usefulness of the proposed work are discussed below.

The on-line condition-monitoring technique has been specifically developed for resonant converters to address the lack of papers in this field. The technique is developed to monitor high-voltage MOSFETs placed on the converter high-side to overcome the limited number and drawbacks of previous work. An innovative approach for measuring the temperature close to the die is developed by placing the sensor close to the die despite the small space in the TO247-4 package. A further advantage of the proposed approach is that it can also be used to characterize different devices at the design stage because,

unlike other works, the OVMC circuit has an output with a constant offset, regardless of the devices used. This feature makes it interesting for device manufacturing companies. In particular, they need an accurate temperature measurement for MOSFETs' characterization and modeling purposes. In detail, the estimation of the MOSFETs switching losses in an LLC converter is difficult due to the energy exchange between the switches occurring during the commutation. However, the accurate measurement of the junction temperature and proper estimation of other power loss contributions (body diode and conduction losses) enables an accurate estimation of the MOSFET losses in the resonant converter. In fact, OVMC is also useful for properly measuring the body diode losses during dead time, as well as the conduction losses, owing to the on-state resistance estimation. Therefore, a proper comparison of different MOSFETs can be performed once an accurate estimation of their losses in an LLC converter can be properly executed. This enables selection of the best device for any LLC application. Moreover, data related to the characterization can be used to improve the accuracy of the device models.

The paper is organized as follows. Section 2 presents the approach used for the MOSFET temperature characterization. Section 3 details the proposed method. Section 4 discusses the issues of condition monitoring in resonant converters and proposes a method to address them. Finally, Section 5 concludes the paper.

2. MOSFET Junction Temperature Characterization

In this paragraph, the preliminary activities concerning the thermal part and the junction temperature measurement will be covered.

The additional small die MOSFET (MD) was soldered near the device under test (DUT), sharing the same TO247-4 package frame to characterize and then validate the junction temperature estimation. The MOSFET MD was configured as a diode, i.e., a shorting gate and source pads, with the backside (drain) of the die soldered onto the package metal frame. Therefore, in the following, this MOSFET is referred to as an MD diode to easily distinguish it from the main MOSFET.

The 4th lead of the TO247-4 package is wire-bonded to the MD die to externally access its anode (pin A in Figure 1). Generally, commercial products with the TO247-4 package have a different pinout and use the 4th as a Kelvin source to optimize the MOSFET switching. In this case, device assembly is performed only to validate the proposed method.

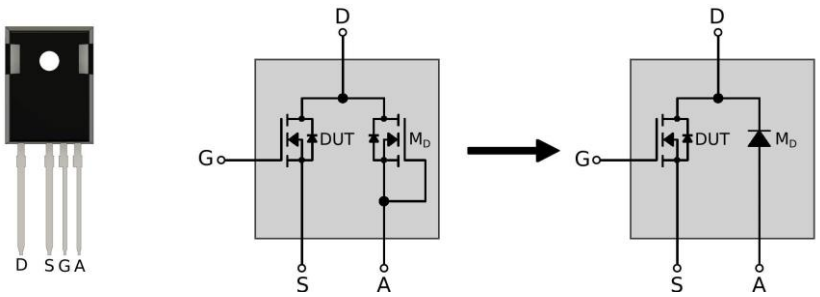

Figure 1. Assembled device with its pinout and internal configuration.

The characterization phase uses the following four measurement steps:

1. MD diode forward voltage vs. temperature,
2. DUT body diode forward voltage vs. temperature,
3. JEDEC 51-14 transient method on DUT,
4. DUT $R_{DS,on}$ characterization vs. temperature.

2.1. MD Diode Characterization

First of all, the MD diode forward voltage is characterized as a function of the temperature at a fixed current (5 mA). This measurement is performed using an analysis tech phase 12 thermal analyzer (Figure 2a) with a calibration bath (Figure 2b), in which the device is

immersed in a uniform-temperature mineral oil bath to collect data over a range of bath temperatures. This relationship is linear, as shown in Figure 2c, and its linear regression (slope equal to −483.6 °C/V and offset equal to 289.3 °C) is used to exploit the diode as a thermal sensor. The mean and maximum errors due to the linear regression are 0.23 °C and 0.66 °C, respectively.

(**a**) (**b**) (**c**)

Figure 2. Analysis tech phase 12 thermal analyzer with results: (**a**) thermal analyzer main unit, (**b**) calibration bath, and (**c**) MD diode forward voltage vs. temperature.

2.2. DUT Body Diode Characterization and JEDEC 51-1

A thermal analyzer was used to apply the JEDEC 51-1 dynamic mode test to the DUT. In general, this method allows us to evaluate the junction-case or junction-ambient thermal resistance of electronic devices, while in this study, it is used to correlate the junction temperatures between the two dices when the DUT is dissipating some amount of power. This method measures the thermal resistance using the following formula:

$$R_{th} = \frac{T_j - T_{amb}}{P_{diss}} \tag{1}$$

where T_j is the junction temperature, T_{amb} is the ambient temperature, and P_{diss} is the power dissipated by the device. Similar to the MD diode, T_j is calculated using the body diode forward voltage characterization vs. temperature at a fixed current I_M.

To measure T_j when the MOSFET is dissipating a certain amount of power through its channel, the body diode should be biased at the current I_M when the MOSFET is active; however, this is not feasible. To solve this problem, the JEDEC 51-1 establishes a dynamic mode in which the thermal system must alternately polarize the MOSFET channel and its body diode. The system waveforms are shown in Figure 3. In the interval t_1, the body diode is polarized at I_M to set the initial condition to find the forward voltage V_{F0} at ambient temperature, which is measured using a thermocouple. During t_2, V_{DS} is set to $V_{H,}$ and the V_{GS} is adjusted to obtain a constant current I_H so as to set the desired dissipated power $P_{diss} = V_H \cdot I_H$. In the interval t_3, the body diode is again polarized at $I_{M,}$ obtaining the junction temperature from the difference between V_{F0} and V_{FSS} and using the slope value of the straight line obtained from the characterization of the body diode. The operations during the intervals t_2 and t_3 are repeated until a thermal steady state is reached. In order to slightly alter the thermal steady state reached during the heating interval t_2, the interval t_3 has to be much smaller than t_2. Usually, t_2 is some tens of seconds; instead t_3 is some tens of milliseconds.

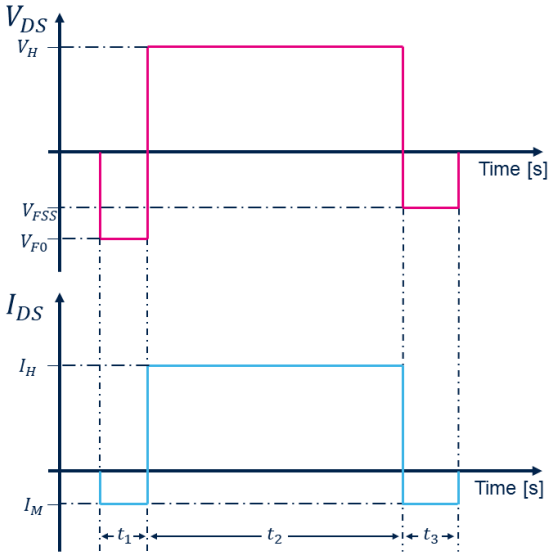

Figure 3. JEDEC 51-1 dynamic mode waveforms with MOSFETs.

This method is normally used to evaluate the thermal resistance while, for this study, it is exploited only for the *Tj* measurement. The test is set with a DUT dissipating power that gradually increases from 0.5 W to 4 W in order to emulate the power that MOSFETs will dissipate in the converter. During this measurement, the MD diode is also polarized at the same current used during the characterization to measure the forward voltage and, therefore, calculate the temperature. This measurement is compared to the DUT junction temperature, obtaining a small difference (<1 °C). This difference is used as a correction factor that relates the temperature measurement obtained through the MD diode to that of the DUT.

2.3. DUT $V_{DS,on}$ Characterization

The following characterization is used to develop the model for estimating the junction temperature by evaluating the drain-source resistance $R_{DS,on}$, which is obtained from the measurement of the drain-source voltage and drain current I_D. To this aim, the $R_{DS,on}$ of the DUTs was characterized versus drain current I_D and junction temperature T_j (Figure 4), as in [23], using the Keysight B1506A curve tracer [24] with an external heater with drain currents up to 20 A.

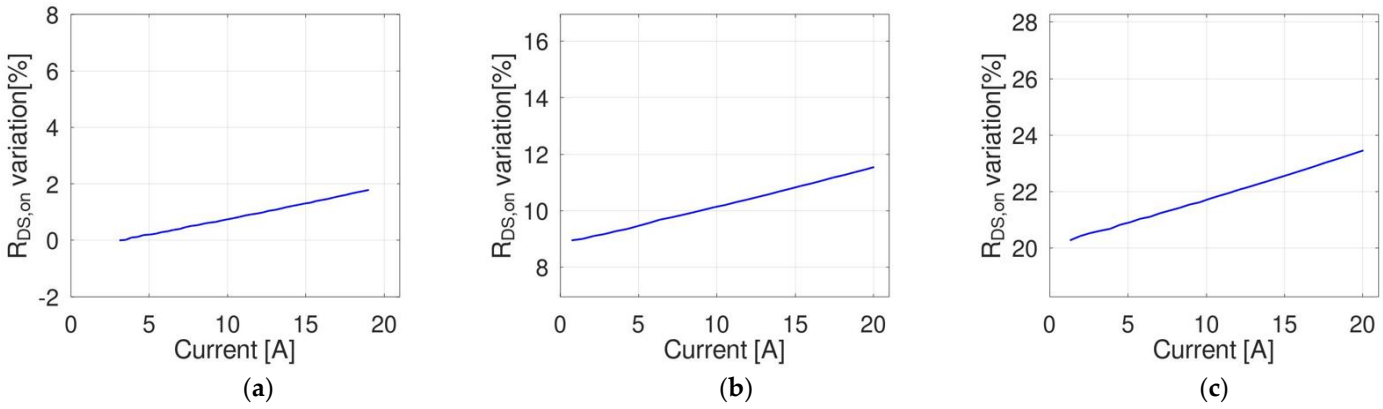

Figure 4. *Cont.*

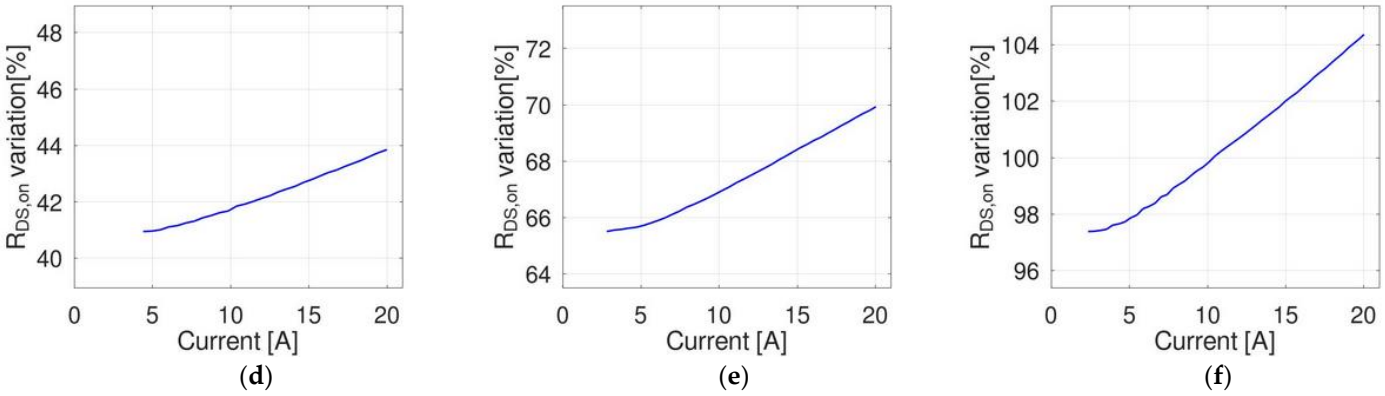

Figure 4. $R_{DS,on}$ characterization with drain current variation at different temperatures: (**a**) 25.5 °C, (**b**) 35.6 °C, (**c**) 50.7 °C, (**d**) 70.9 °C, (**e**) 92.8 °C, (**f**) 120.7 °C.

In this step, the temperature was measured through the M_D diode using the previous characterization, without considering the previous correction factor. This factor is not necessary because the temperature is imposed by the heater, and consequently, the MD diode and DUT are in thermal equilibrium. These $R_{DS,on}$ measurements, are used to obtain T_j as a function of $R_{DS,on}$ and I_D. The regression used is the following 2nd order polynomial function:

$$T_j(R_{DS,on}, I_D) = a_1 + a_2 \cdot R_{DS,on} + a_3 \cdot R_{DS,on}^2 + a_4 \cdot I_D + a_5 \cdot R_{DS,on} \cdot I_D \quad (2)$$

with $a_1, \ldots, a_5$ are the polynomial coefficients of the function, equal to, respectively, −117.4573, 3229.3406, −8725.5927, 0.0043993, −2.6674.

The resulting function is illustrated in Figure 5. This function was mathematically validated using the results shown in Figure 4. Figure 6 shows the temperature estimated (blue circle) for different junction temperatures (green line). Table 1 reports, for each temperature, the maximum error together with the current at which the maximum error occurs.

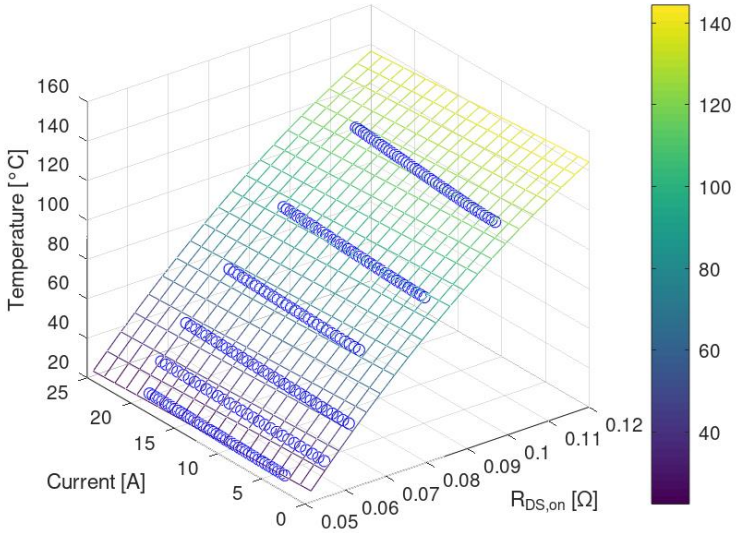

Figure 5. Temperature regression as a function of $R_{DS,on}$, and I_D. The blue circles represent the measured values.

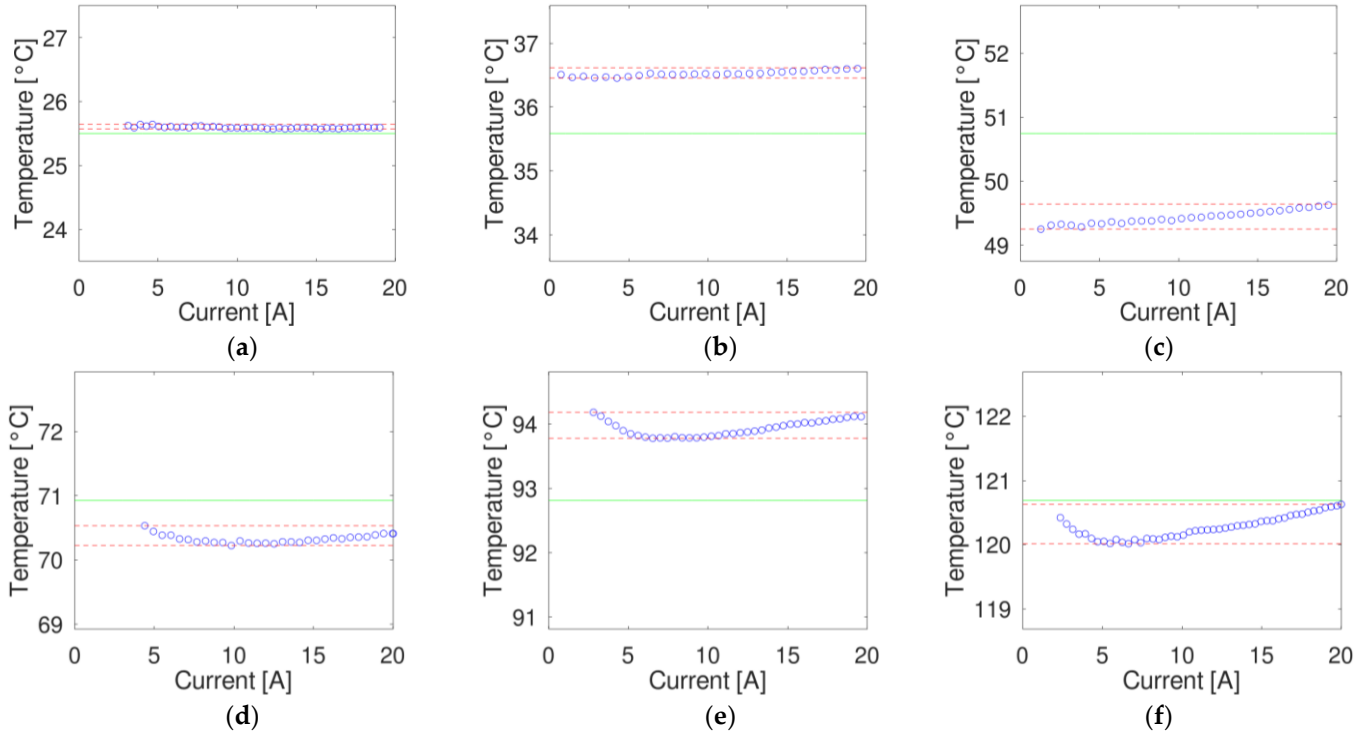

Figure 6. Temperature estimated using Equation (2), the values of $R_{DS,on}$, and I_D reported in Figure 4 (blue circles) vs. the actual temperature (green). The red dotted lines indicate the minimum and maximum errors. (**a**) 25.5 °C, (**b**) 35.6 °C, (**c**) 50.7 °C, (**d**) 70.9 °C, (**e**) 92.8 °C, (**f**) 120.7 °C.

Table 1. Temperature estimation maximum error and related current for different temperatures.

Actual Temperature (°C)	Maximum Error (°C)	Current at which the Maximum Error Occurs (A)
25.5	0.14	4.6
35.6	1.03	20
50.7	1.5	1.3
70.9	0.7	9.8
92.8	1.37	2.8
120.7	0.67	6.6

3. Evaluation of the On-State Resistance Used for Junction Temperature Estimation

3.1. On-Voltage Measurement Circuit

The value of $R_{DS,on}$ can be estimated from the relationship between on-state voltage and current measurements. A Tektronix TCP0030A current probe has been used for the current measurement. The use of an oscilloscope and high-voltage probe to measure the on-state voltage in a high-voltage circuit leads to inaccurate values. Therefore, an on-state voltage measurement circuit (OVMC) is required [14]. The output of the OVMC (V_m) limits the V_{DS} voltage variation (Figure 7) to improve the accuracy of the voltage measurement by setting a smaller vertical scale.

The measurement of the on-state voltage presents several challenges in terms of accuracy and high blocking voltage capability. Moreover, the high switching frequencies of modern power devices require an extremely fast dynamic response.

In the half-bridge (HB) LLC, the MD diode was not used as the thermal sensor of the low-side (LS) MOSFET because of the drain voltage; consequently, the MD cathode potential swings from 0 V to the BUS voltage (400 V). The voltage transient at the middle point, associated with the stray elements, is considered a potential source of noise. For this reason, the measurement of the voltage with MD was performed only for the high-side

(HS) MOSFET where the MD cathode voltage is fixed at V_{BUS}. Therefore, the OVMC circuit has been designed for the HS MOSFET. The OVMC final circuit is shown in Figure 8.

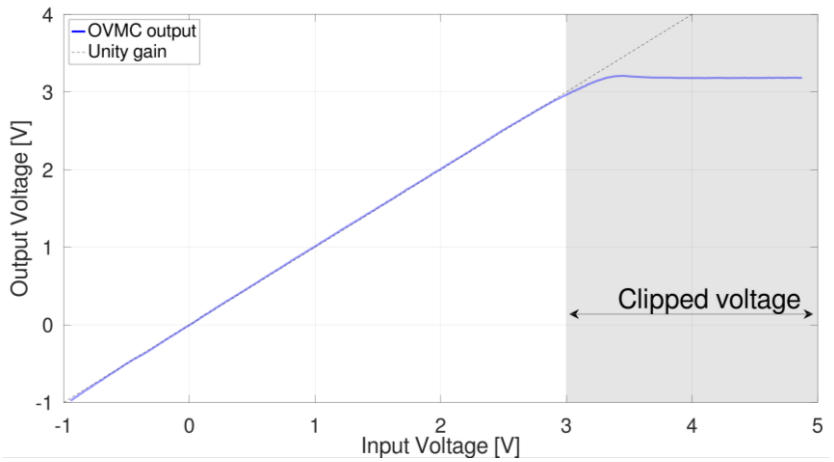

Figure 7. OVMC output vs. input voltage.

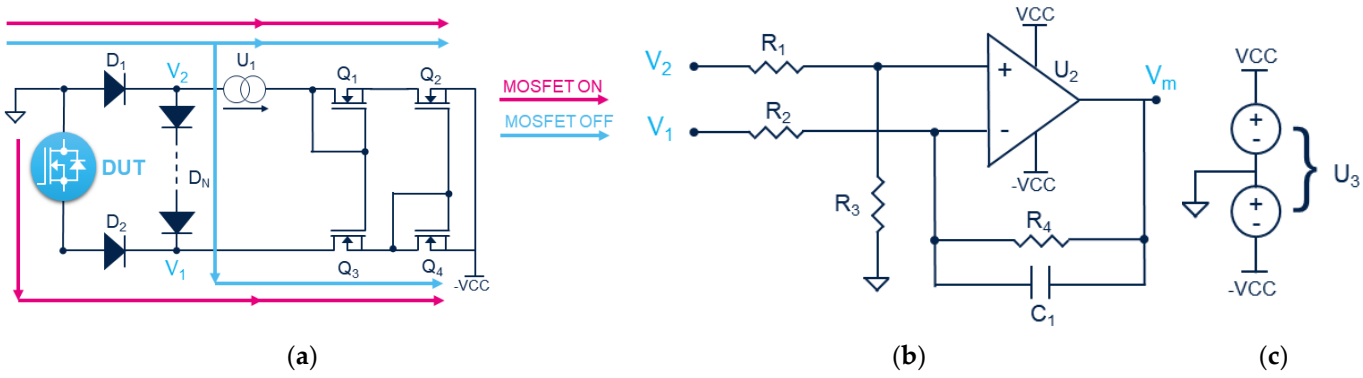

(**a**) (**b**) (**c**)

Figure 8. Proposed OVMC: (**a**) main circuit and stages of operation, (**b**) operational amplifier circuit, and (**c**) power circuit.

Table 2 reports the characteristics and values of the devices used. The OVMC with these devices presents a 600 V maximum drain voltage. To increase this voltage is sufficient to choose D_1 and D_2 diodes with a higher voltage or insert more diodes in series or, in other types of circuits, increase the number of clamping stages [25].

The basic circuit is proposed in [26,27] but, in this study, several changes have been made. The schematic has been mirrored to have a reference point on the drain rather than on the source [12,13,18]. Moreover, transistors Q_1, Q_2, Q_3, and Q_4 are MOSFET instead of BJTs and form a Wilson current mirror instead of a cascode mirror. Finally, the biasing resistor has been replaced with a constant current driver.

The diode D_1 is always polarized by U_1 at about 10 mA. When the DUT is ON, D_2 is polarized with the same current as D_1 owing to the current mirror (purple line in Figure 8a), and when the DUT is OFF, the series of diodes D_N is polarized with the same current as U_1 (light blue line in Figure 8a). The number of diodes, D_N, changes based on the application and MOSFET $R_{DS,on}$ and define the clamp voltage of the OVMC. In this work, there are six diodes.

Table 2. OVMC components.

Devices	Part Number	Description	Parameter	Value
D_1, D_2	RFU02VSM6STR	Super fast recovery diode	Repetitive peak reverse voltage Average current Typ. Forward voltage Capacitance at V_R = 0	600 V 0.2 A 1.5 V 5 pF
D_N	RF05VAM2STR	Super fast recovery diode	Repetitive peak reverse voltage Average current Typ. Forward voltage Capacitance at V_R = 0l	200 V 0.5 A 0.85 V 25 pF
U_1	NCR420U	LED/diode driver	Maximum enable voltage Typ. stabilized output current	40 V 10 mA
U_2	THS4631D	High-voltage, high slew rate, wideband Operational Amplifier	Unity gain bandwidth Slew rate Max. supply voltage Max. Input Bias Current Input Voltage Noise Input Offset Voltage	325 MHz 900 V/µs 33 V 100 pA 7 nV/$\sqrt{Hz}$ 500 µV
U_3	PESE1-S5-D12-M-TR	Isolated dual-output DC-DC converter	Input voltage Output voltage Max. output current Max. output power	5 V ±12 V ±42 mA 1 W
$Q_{1–4}$	2N7002	N-channel MOSFET	Max. Drain—Source Voltage Max. continuous Drain current Typ. Gate threshold voltage Typ. Turn-On time Typ. Turn-Off time	60 V 200 mA 2.1 V 20 ns 15 ns
$R_{1–4}$		Resistors	Resistance	1 kΩ
C_1		Capacitor	Capacitance	5 pF

The op-amp circuit (Figure 8b) is a differential stage that provides the difference between V_2 and V_1; therefore, during the on-state, the output V_m is:

$$V_m = V_2 - V_1 = -V_{D1} - (-V_{DS,on} - V_{D2}) \quad (3)$$

Considering that D_1 and D_2 are polarized in the same way, i.e., $V_{D1} \approx V_{D2}$, then:

$$V_m = V_{DS,on} \quad (4)$$

Therefore, the OVMC output is $V_{DS,on}$ plus an offset due to op-amp and a slight difference between the diodes' forward voltage V_D.

An isolated dual-output 12V DC-DC converter (Figure 8c) is used to supply the OVMC board. An isolated converter permits to follow the V_{DS} signal better, avoiding a voltage drop on the drain line. Unlike in [28], where there is an active circuit to subtract this voltage.

An important challenge when reading the OVMC output V_m is that this signal refers to the drain voltage of HS MOSFET, which is usually connected to the input voltage. To read this voltage, a low-voltage differential probe with a high common mode voltage must be used. Usually, low-voltage differential probes have low common mode voltages unless an opto-isolated probe is used [27]. To avoid this problem, the oscilloscope ground is connected to the drain reference in order to cancel the common mode voltage of the low-voltage differential probe, as shown in Figure 9.

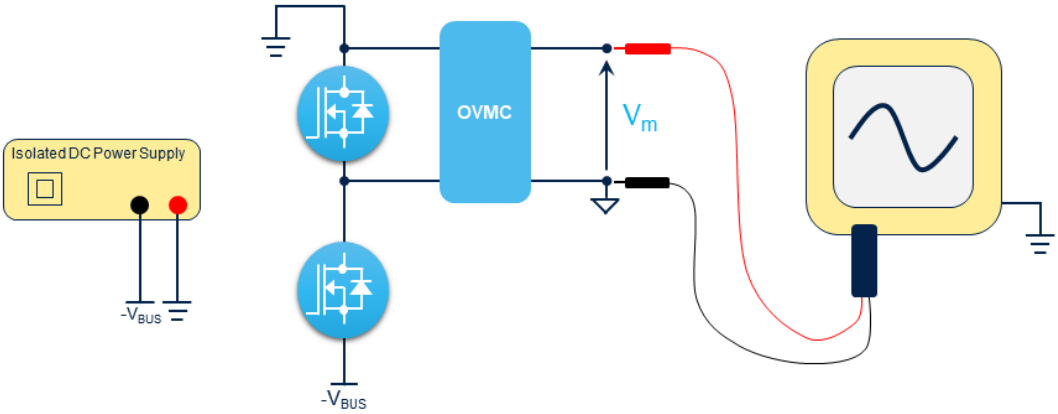

Figure 9. Ground connection between the half-bridge board and oscilloscope. NOTE: V_{BUS} power supply is isolated from the ground.

Moreover, the OVMC allows for accurately measuring the power dissipated on the body diode (in ZVS converter) and the conduction losses of the MOSFET; therefore, a further characteristic of OVMC is that of being able to read both positive and negative voltage, unlike the circuit proposed in [25].

3.2. LLC Converter

In this work, condition monitoring is applied to a resonant converter in the telecom market. Therefore, the OVMC was adopted in a 1500 W LLC converter. This type of converter has been chosen as the current changes its polarity; the zero-crossing point is fundamental for the calibration, as will be explained later.

A typical LLC converter for the telecom market with the following characteristics has been realized:

- Input voltage: 400 V ± 1%
- Maximum output power: 1500 W
- Output voltage: 48 V ± 1%
- Maximum output current: 31.25 A
- Efficiency (at maximum load): ≥95%
- Resonant frequency: 102.73 kHz

LLC converter is a high-power buck converter. In this case, a half-bridge converter is used, and its schematic is shown in Figure 10a. The two MOSFETs Q_1 (high-side HS) and Q_2 (low-side LS) commutate at a high frequency with the same on-time T_{ON}. The operation exploits the resonance of LLC circuits, which are composed of L_R, L_M, and C_R.

The output voltage is determined by the following formula:

$$V_{out} = M_g \cdot \frac{1}{n} \cdot \frac{V_{in}}{2} \tag{5}$$

where M_g is the gain of the LLC tank, which depends on the switching frequency, and n is the transformer turns ratio. The switching frequency changes to the right of the gain curve peak, as shown in Figure 10b, and as it approaches the curve peak, the output power increases. Working on the right side of the curve allows us to achieve zero voltage switching (ZVS) conditions during turn-on.

Figure 11 shows a typical LLC converter switching period with V_{DS}, OVMC output V_m, and the three MOSFET operating areas. During dead time, the body diode conducts, which permits it to reach ZVS (blue area). After that, the MOSFET turn-on occurs, and the current passes through its channel with a drain voltage that follows the current shape (yellow area). Finally, the MOSFET is turned off (green area), and the complementary MOSFET follows the behavior related to the blue area. At low power, the current shape

is triangular, and once the frequency approaches the peak of the gain curve, the current becomes sinusoidal.

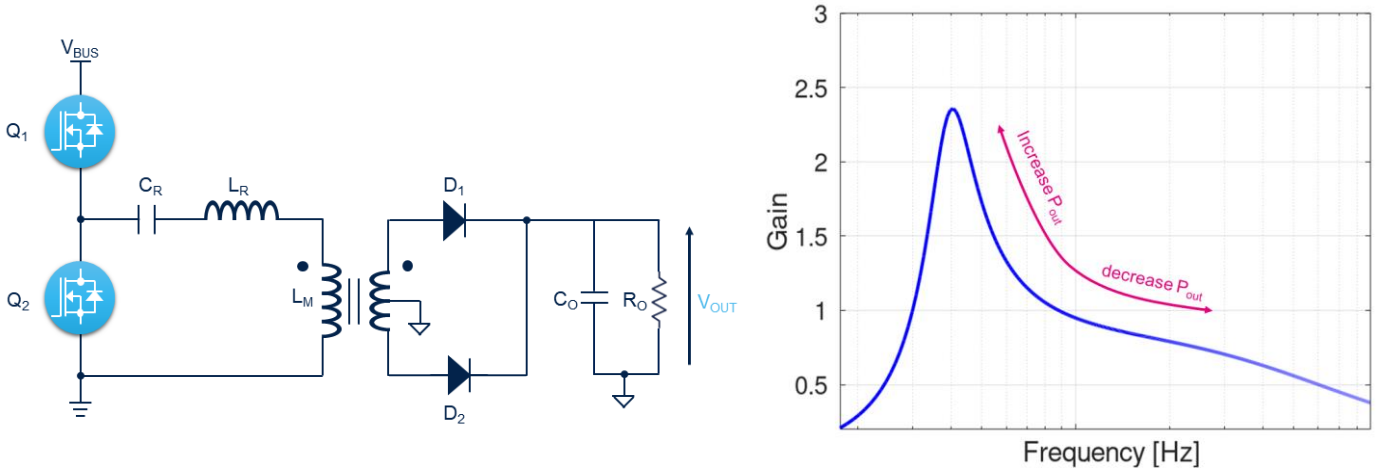

(**a**) (**b**)

Figure 10. Half-Bridge LLC converter: (**a**) schematic and (**b**) gain curve.

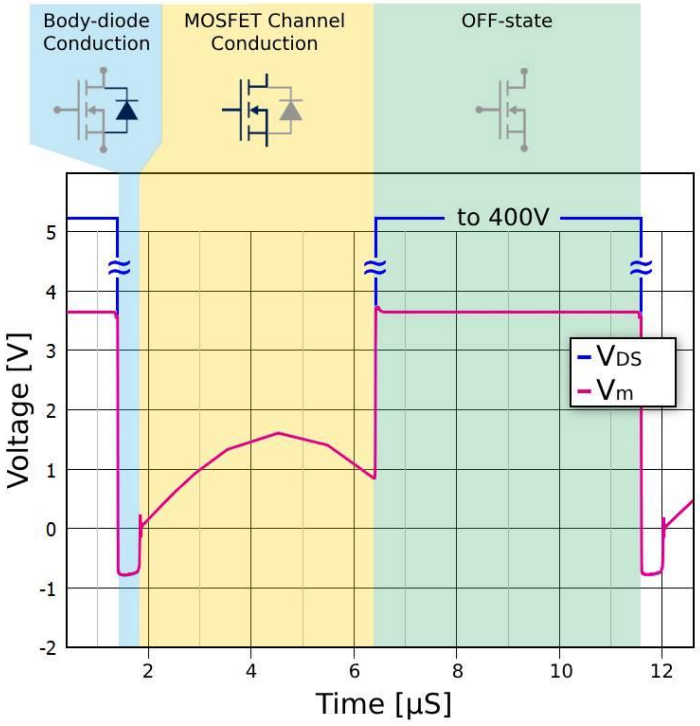

Figure 11. Typical LLC converter switching period V_{DS} with OVMC output V_m and highlighted MOSFET operating area.

3.3. OVMC Compensation in LLC Converter

Due to the non-idealities of the operational amplifier and resistors, the gain is not unitary. To evaluate the actual value, the V_{DS} input of the OVMC is connected to a waveform generator that generates a triangular waveform. By comparing this input signal with the V_m output signal from the clipped zone, the real gain can be calculated, from which a corrective factor to account for the oscilloscope measurements is obtained.

The OVMC measures the on-state voltage across the DUT leads. Therefore, the V_m voltage is equal to $V_{DS,on}$ plus the voltage across the parasitic inductance of the DUT wire bonding and leads [29]. For this reason, the OVMC must be soldered close to the package,

as shown in Figure 12a. The different contributions are shown in Figure 12b, where $L_{PCB,D}$ and $L_{PCB,S}$ incorporate the drain and source stray inductance of the PCB trace, connectors, and DUT leads, while $L_{stray,D}$ and $L_{stray,S}$ represent the drain and source stray inductances. The latter contributions are indistinguishable, and consequently, they are considered as a whole parasitic inductance L_{stray}:

$$L_{stray} = L_{stray,D} + L_{stray,S} \tag{6}$$

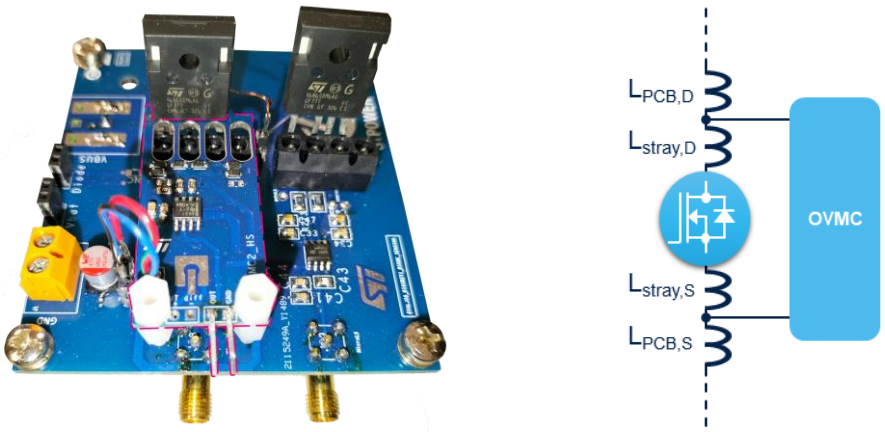

(**a**) (**b**)

Figure 12. HB board prototype. (**a**) OVMC board on prototype (**b**) representation of DUT and board parasitic inductances with OVMC connection.

Moreover, V_m also includes a small offset due to either the operational amplifier stage or the differential probe Tektronix TDP1500 used. To compensate for the extra voltage caused by L_{stray}, it is subtracted mathematically using an oscilloscope.

$$V_{DS,on} = V_m - V_{offset} - L_{stray}\frac{dI_D}{dt} \tag{7}$$

The quantity L_{stray} can be obtained by physical simulations or experimental waveforms. In order to obtain a resistive load, I_D and $V_{DS,on}$ must be in phase, and therefore, the zero-crossing of the current and voltage must coincide. As shown in Figure 13a, the zero-crossing of I_D does not coincide with that of V_m. Therefore, L_{stray} and V_{offset} can be extracted from waveforms at two different converter power levels P_1 and P_2. Changing the output power level, the dI_D/dt also changes, and therefore, it is possible to distinguish V_{offset} from $L_{stray}\frac{dI_D}{dt}$ as follows.

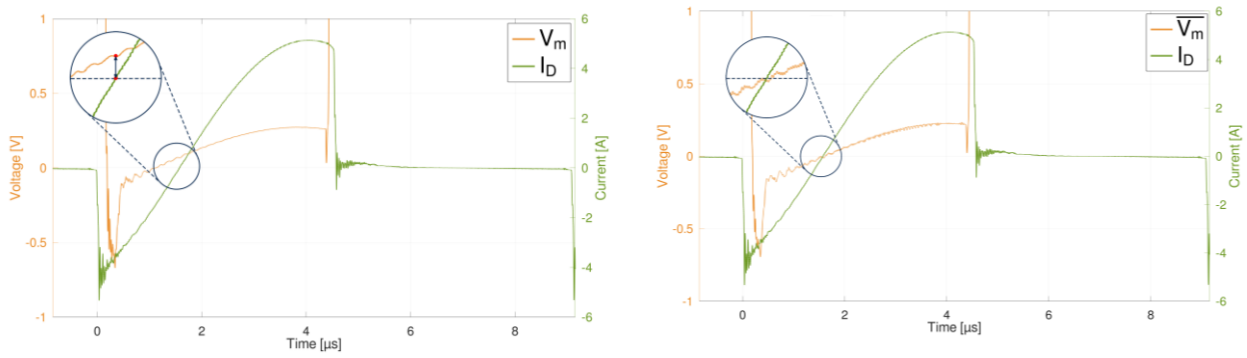

(**a**) (**b**)

Figure 13. LLC waveforms. Drain current in green, V_m output in yellow. (**a**) without OVMC compensation and (**b**) with OVMC compensation.

For the first output level $P_{out} = P_1$, the V_m signal at $I_D = 0$ is

$$V_m^{(1)}|_{I_D=0} = V_{offset} + L_{stray}\frac{dI_D^{(1)}}{dt} \tag{8}$$

where $V_m|_{I_D=0}$ and dI_D/dt can be measured with an oscilloscope, and thus, they will be the known terms.

For the second output level $P_{out} = P_2$, in the same way, it can be written as

$$V_m^{(2)}|_{I_D=0} = V_{offset} + L_{stray}\frac{dI_D^{(2)}}{dt} \tag{9}$$

In this way a system with two equations and two unknowns can be obtained as

$$\begin{cases} V_m^{(1)}|_{I_D=0} = V_{offset} + L_{stray}\frac{dI_D^{(1)}}{dt}, & P_{out} = P_1 \\ V_m^{(2)}|_{I_D=0} = V_{offset} + L_{stray}\frac{dI_D^{(2)}}{dt}, & P_{out} = P_2 \end{cases} \tag{10}$$

Solving the system provides the value of V_{offset} and L_{stray}. The compensated $\overline{V_m}$ voltage is

$$\overline{V_m} = V_m - V_{offset} - L_{stray}\frac{dI_D}{dt} \tag{11}$$

In this way, V_{offset} accounts for the OVMC, the differential voltage probe, and the current probe offset voltages. In the prototype, $L_{stray} \approx 9nH$.

The waveform with this correction is shown in Figure 13a, highlighting the in-phase current and voltage. Figure 14a,b show the waveforms at full load without and with this correction. Under this condition, the converter operates in a quasi-sinusoidal steady state, and consequently, the lack of correction also leads to a shift in the voltage peak relative to the current peak.

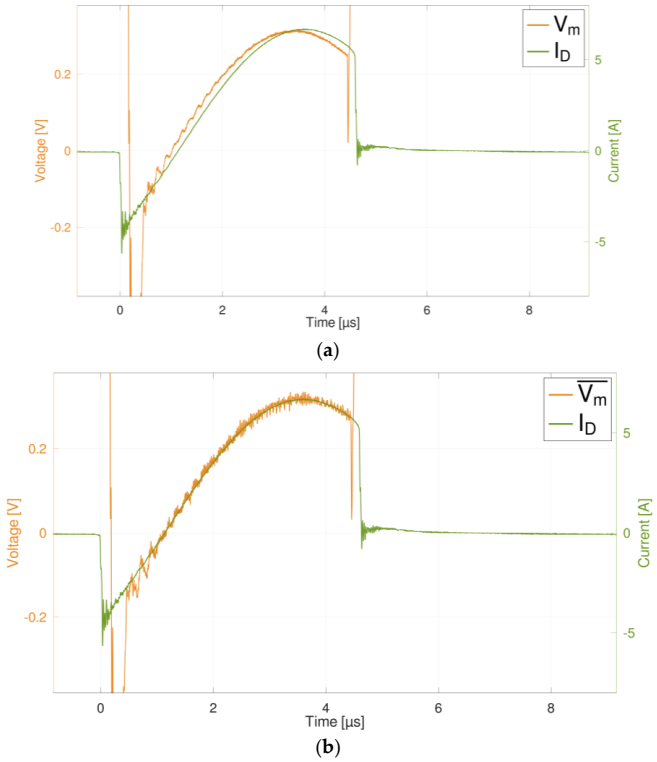

Figure 14. LLC waveforms at full load. Drain current in green, V_m output in yellow. (**a**) without OVMC compensation and (**b**) with OVMC compensation.

4. Condition Monitoring of the Resonant Converter by Combining the MOSFET Junction Temperature Characterization and OVMC

The MOSFETs used in this LLC converter are two STWA46N65DM6, 650 V devices with $R_{DS,on(typ)}$ = 55 mΩ. The compensation techniques described previously are extremely important in this case because the low $R_{DS,on}$ could lead to inaccurate on-state voltage measurement since it is small. The MOSFET $R_{DS,on}$ is directly evaluated using the oscilloscope Tektronix MSO66B that measures $\overline{V_m}$ and I_D (Figure 15a). The light blue waveform in Figure 15 represents the $R_{DS,on}$ and it diverges when I_D approaches zero, as division by zero is carried out. This divergence causes an oscillation, and therefore, the $R_{DS,on}$ value is calculated after damping by the mean value between the two dashed lines. The measured $R_{DS,on}$ vs. P_{OUT} is shown in Figure 15b. From the inspection of Figure 15a, it is apparent that possible V_m spikes and oscillations during the switching transient do not affect the estimation because they are executed inside the MOSFET conduction interval (inside the dashed lines). Moreover, these spikes and oscillations do not affect circuit operation because they do not exceed the components' safe-operating-area.

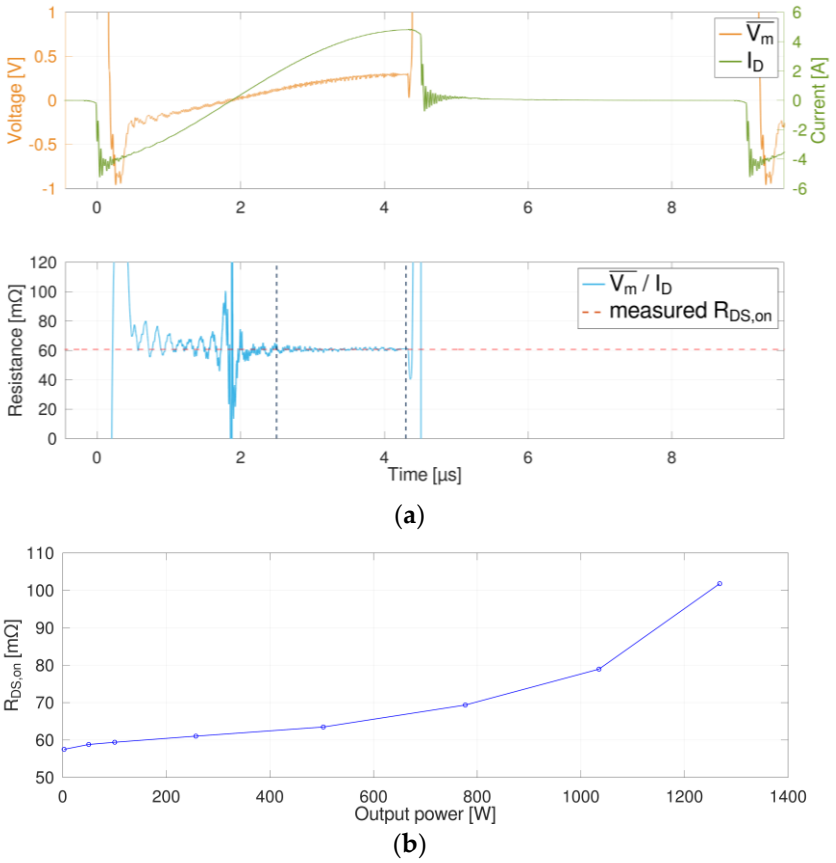

Figure 15. $R_{DS,on}$ evaluation (**a**) LLC waveforms at 250 W: Drain current in green, $\overline{V_m}$ output in yellow, $\overline{V_m}/I_D$ in light blue, measured $R_{DS,on}$ in red dashed line. (**b**) $R_{DS,on}$ variation as a function of the LLC output power.

As previously mentioned, to validate the temperature estimation through resistance measurement, a diode was inserted inside the package. As the MD cathode is connected to the DUT drain, V_f cannot be measured at the drain lead because it also includes the voltage drop at the drain lead caused by the current flowing on the DUT MOSFET. To avoid this problem, an additional wire is soldered onto the frame behind the M_D die.

The MD diode is polarized at a 5 mA current with an LD1117STR based circuit with a constant current configuration. The MD V_f was monitored with a Keithley DMM6500 6.5-digit multimeter (Tektronix, Beaverton, OR, USA) running a dedicated script that instantly converted the measured voltage into temperature (Figure 16).

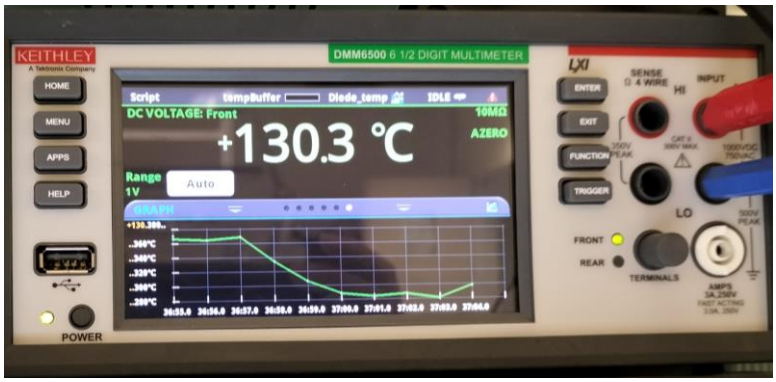

Figure 16. Keithley DMM6500 multimeter running the custom script.

In the beginning, V_f is associated with ambient temperature measured through a thermocouple. Then, the correction factor described in Section 2.1 is used to relate the diode temperature with the DUT junction temperature. Finally, the temperature has been calculated using the previous characterization of the MD diode forward voltage vs. temperature reported in Figure 2c.

Equation (2) is used to estimate T_j from the $R_{DS,on}$ measurement, as shown in Figure 17, considering two different output power levels. In detail, Equation (2) is calculated using the oscilloscope (brown waveform), and the mean of the values between the two vertical dashed lines is the estimated T_j, called T_{RDS}, and is indicated by the red dashed lines. In Figure 17, the temperature calculated between the cursors is almost constant, thus confirming the goodness of the regression function for all current shapes and at different LLC converter output powers.

During the LLC converter operation, P_{out} gradually increased, and the measurements were acquired at a thermal steady state. The measurements were halted when the MOSFETs were overheated at 120 °C. The T_{RDS} results compared to the temperature measured by the MD diode are shown in Figure 18. The figure shows a ΔT of 0.35 °C as the maximum error between the two measures.

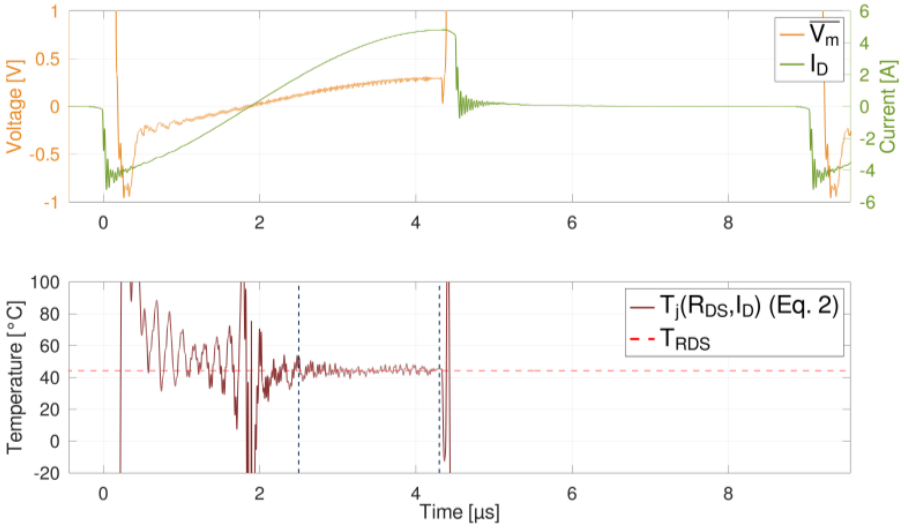

(**a**)

Figure 17. *Cont.*

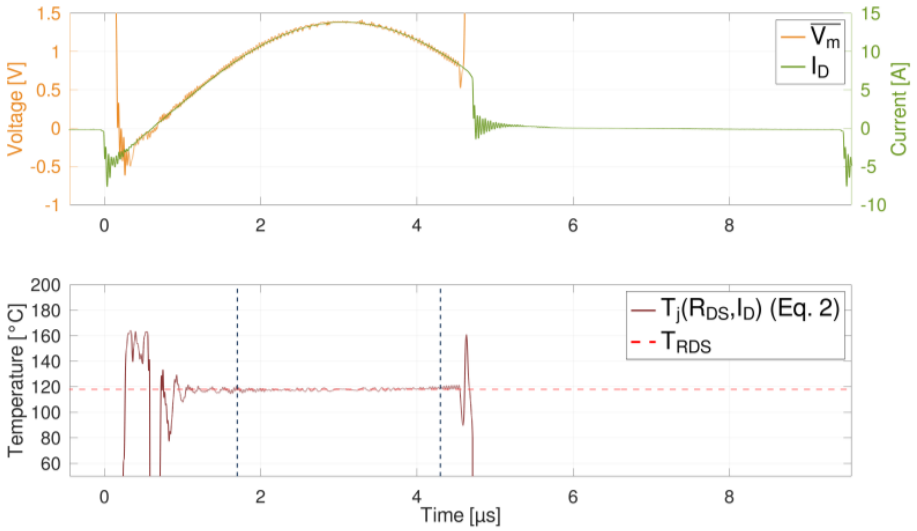

(**b**)

Figure 17. LLC waveforms at two power levels: (**a**) 250 W and (**b**) 1280 W. Drain current in green, $\overline{V_m}$ output in yellow, T_j estimated using Equation (2) in brown, and calculated T_{RDS} in a red dashed line.

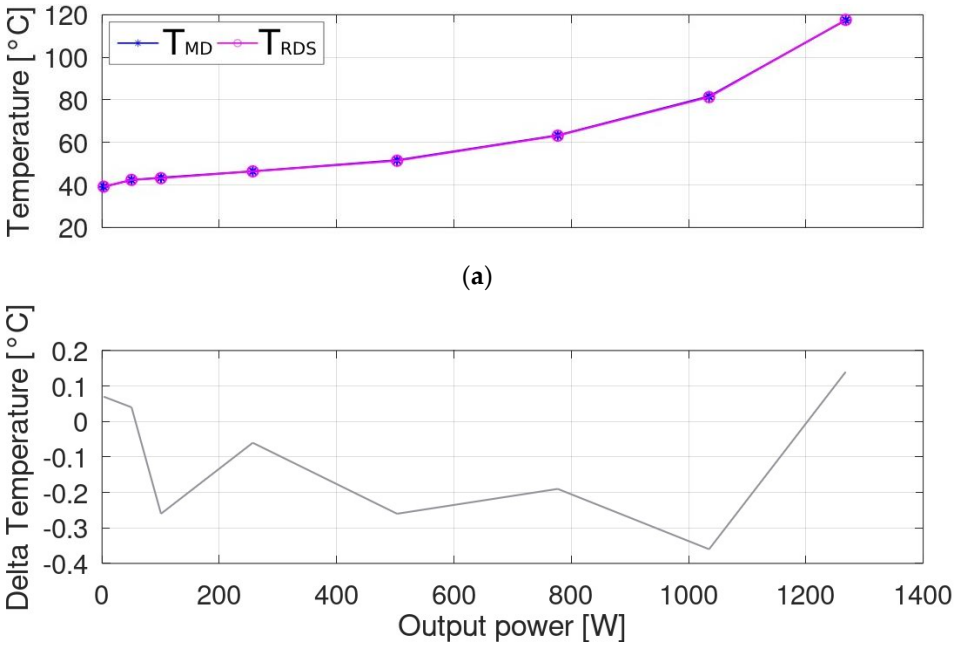

(**a**)

(**b**)

Figure 18. Comparison between the value of *Tj* estimated using the proposed approach based on the $R_{DS,on}$ measurement and the reference one evaluated by means of the MD diode. (**a**) *Tj* estimation at different resonant converter power outputs. (**b**) Difference between the two estimations.

5. Conclusions

In the semiconductor industry, the junction temperature in a MOSFET is directly obtained through the thermal characterization of its body diode, as established by JEDEC 51–14. This measurement is not practical when the MOSFET operates in a resonant converter. In this work, the MOSFET junction temperature was measured using two approaches. One is based on the variation in the forward voltage of a diode (direct method), and the other exploits the electrical measurements obtained through an OVMC (indirect method). Starting from electrical measurements, the proposed method based on the OVMC allows us to track the HS MOSFET junction temperature while an LLC power converter is running. The junction

temperature derived using this indirect method was compared with that derived using the direct method and considered as a reference because it exploits a simultaneous thermal value retrieved from an additional MOSFET housed inside the same package used as a thermal sensor.

The junction temperature estimation of OVMC was compared with that of the direct method for accuracy verification. The results confirm the effectiveness of the proposed approach (maximum error of less than 1%).

The proposed approach is simpler because it can be applied to any MOSFET without the need for specific assemblies. Furthermore, the OVMC refers exactly to the junction temperature of the die under test, while the diode method measures the temperature of a die near the DUT.

Furthermore, the use of the OVMC allows monitoring of the junction temperature during any operating condition of the resonant converter. Hence, condition monitoring anticipates the potential risks of MOSFET failure. An additional advantage is the on-line monitoring of the $R_{DS,}$ which enables the identification of potential degradation and aging of the MOSFET, and then performs predictive maintenance. Another advantage is the potential use of OVMC to measure conduction losses and body diode losses. Therefore, this technique can also be used for characterization and modeling of MOSFETs operating in resonant converters.

Author Contributions: Conceptualization, M.V. and A.S.; Data curation, M.V. and G.S.; Formal analysis, A.S.; Investigation, G.B.; Methodology, M.V., A.S. and F.I.; Supervision, A.S. and S.A.R.; Validation, G.S.; Visualization, M.V.; Writing—original draft, M.V. and A.S.; Writing—review & editing, M.V., F.I. and S.A.R. All authors have read and agreed to the published version of the manuscript.

Funding: This research received no external funding.

Data Availability Statement: Data are contained within the article.

Conflicts of Interest: Marco Ventimiglia, Alfio Scuto, Giuseppe Sorrentino, and Gaetano Belverde were employed by the company ST Microelectronics Co., Ltd. Francesco Iannuzzo and Santi Agatino Rizzo declare that the research was conducted in the absence of any commercial or financial relationships that could be construed as potential conflicts of interest.

References

1. Kumar, A.; Moradpour, M.; Losito, M.; Franke, W.-T.; Ramasamy, S.; Baccoli, R.; Gatto, G. Wide Band Gap Devices and Their Application in Power Electronics. *Energies* **2022**, *15*, 9172. [CrossRef]
2. Rizzo, S.A.; Salerno, N. Actual reasons involving turn-off losses improvement with increasing load and gate resistance in MOSFETs enhanced with Kelvin source. *IEEE Trans. Ind. Electron.* **2024**, *71*, 369–379. [CrossRef]
3. Roccaforte, F.; Fiorenza, P.; Greco, G.; Nigro, R.L.; Giannazzo, F.; Iucolano, F.; Saggio, M. Emerging trends in wide band gap semiconductors (SiC and GaN) technology for power devices. *Microelectron. Eng.* **2018**, *187–188*, 66–77. [CrossRef]
4. Adragna, C. LLC Resonant Converters: An Overview of Modeling, Control and Design Methods and Challenges. *Found. Trends® Electr. Energy Syst.* **2022**, *5*, 75–491. [CrossRef]
5. Nguyen, M.H.; Kwak, S. Enhance Reliability of Semiconductor Devices in Power Converters. *Electronics* **2020**, *9*, 2068. [CrossRef]
6. Martínez, J.; Riba, J.-R.; Moreno-Eguilaz, M. State of Health Prediction of Power Connectors by Analyzing the Degradation Trajectory of the Electrical Resistance. *Electronics* **2021**, *10*, 1409. [CrossRef]
7. Rizzo, S.A.; Susinni, G.; Iannuzzo, F. Intrusiveness of Power Device Condition Monitoring Methods: Introducing Figures of Merit for Condition Monitoring. *IEEE Ind. Electron. Mag.* **2022**, *16*, 60–69. [CrossRef]
8. Bayerer, R.; Herrmann, T.; Licht, T.; Lutz, J.; Feller, M. Model for Power Cycling lifetime of IGBT Modules—Various factors influencing lifetime. In Proceedings of the 5th International Conference on Integrated Power Electronics Systems, Nuremberg, Germany, 11–13 March 2008; pp. 1–6.
9. Junghaenel, M.; Schmidt, R.; Strobel, J.; Scheuermann, U. Investigation on Isolated Failure Mechanisms in Active Power Cycle Testing. In Proceedings of the PCIM Europe 2015; International Exhibition and Conference for Power Electronics, Intelligent Motion, Renewable Energy and Energy Management, Nuremberg, Germany, 19–20 May 2015; pp. 1–8.
10. Duan, Y.; Kang, J.; Shi, Y.; Xin, Z. An Online On-State Voltage Measurement Circuit With Series Diode Clamp for SiC MOSFETs. *CPSS Trans. Power Electron. Appl.* **2023**, *8*, 23–32. [CrossRef]
11. Baker, N.; Luo, H.; Iannuzzo, F. Simultaneous On-State Voltage and Bond-Wire Resistance Monitoring of Silicon Carbide MOSFETs. *Energies* **2017**, *10*, 384. [CrossRef]

12. Hosseinabadi, F.; Jaman, S.; Bhoi, S.K.; Hasan, M.M.; Chakraborty, S.; El Baghdadi, M.; Hegazy, O. Implementation of onsite Junction Temperature Estimation for a SiC MOSFET Module for Condition Monitoring. In Proceedings of the 2022 24th European Conference on Power Electronics and Applications (EPE'22 ECCE Europe), Hanover, Germany, 5–9 September 2022; pp. P.1–P.6.
13. Hong, K.; Chen, X.Y.; Chen, Y.; Zhang, M.S.; Wang, J.L.; Jiang, S.; Pang, Z.; Yang, H.M.; Xue, N.; Gou, H.Y.; et al. Experimental Investigations Into Temperature and Current Dependent On-State Resistance Behaviors of 1.2 kV SiC MOSFETs. *IEEE J. Electron Devices Soc.* **2019**, *7*, 925–930. [CrossRef]
14. Zhang, Q.; Zhang, P. A Novel Model of the Aging Effect on the ON-State Resistance of SiC Power MOSFETs for High-Accuracy Package-Related Aging Evaluation. *IEEE Trans. Ind. Electron.* **2023**, *70*, 9495–9504. [CrossRef]
15. Zhang, Q.; Yang, Y.; Zhang, P. A Novel Method for Monitoring the Junction Temperature of SiC MOSFET On-line Based on On-state Resistance. In Proceedings of the 2019 22nd International Conference on Electrical Machines and Systems (ICEMS), Harbin, China, 11–14 August 2019; pp. 1–5.
16. Ye, Z.; Zheng, Z.; Li, C. A New Measurement of Online Junction Temperature Based on On-state Resistance. In Proceedings of the 2023 IEEE 6th International Electrical and Energy Conference (CIEEC), Hefei, China, 12–14 May 2023; pp. 3367–3370.
17. Stella, F.; Pellegrino, G.; Armando, E.; Daprà, D. Online Junction Temperature Estimation of SiC Power MOSFETS through On-State Voltage Mapping. *IEEE Trans. Ind. Appl.* **2018**, *54*, 3453–3462. [CrossRef]
18. Magnone, P.; Petucco, A.; Thevenet, N.; Abedini, H. Simplified on-line monitoring system of MOSFET on-resistance based on a semi-empirical model. In Proceedings of the 2019 IEEE Applied Power Electronics Conference and Exposition (APEC), Anaheim, CA, USA, 17–21 March 2019; pp. 2746–2750.
19. Sirat, A.P.; Roy, C.; Evans, D.; Gafford, J.; Parkhideh, B. In-Situ Ultrafast Sensing Techniques for Prognostics and Protection of SiC Devices. In Proceedings of the 2022 IEEE 9th Workshop on Wide Bandgap Power Devices & Applications (WiPDA), Redondo Beach, CA, USA, 7–9 November 2022; pp. 142–147.
20. Roy, C.; Kim, N.; Evans, D.; Sirat, A.P.; Gafford, J.; Parkhideh, B. A Half-Bridge On-State Voltage Sensor for In-Situ Measurements. In Proceedings of the 2022 IEEE Energy Conversion Congress and Exposition (ECCE), Detroit, MI, USA, 9–13 October 2022; pp. 1–7.
21. Roy, C.; Kim, N.; Gafford, J.; Parkhideh, B. On-State Voltage Measurement of High-Side Power Transistors in Three-Phase Four-Leg Inverter for In-Situ Prognostics. In Proceedings of the 2021 IEEE Energy Conversion Congress and Exposition (ECCE), Vancouver, BC, Canada, 10–14 October 2021; pp. 2770–2776.
22. Scuto, A.; Sorrentino, G.; Ventimiglia, M.; Belverde, G.; Nardo, D.; Vitale, G.; Lullo, G. Assessment of MOSFET switching losses in an LLC converter by a calorimetric method. In Proceedings of the 2023 IEEE Applied Power Electronics Conference and Exposition (APEC), Orlando, FL, USA, 19–23 March 2023; pp. 2456–2462.
23. Zhang, Q.; Lu, G.; Yang, Y.; Zhang, P. A High-Frequency Online Junction Temperature Monitoring Method for SiC mosfets Based on on-State Resistance With Aging Compensation. *IEEE Trans. Ind. Electron.* **2023**, *70*, 7393–7405. [CrossRef]
24. B1506A Power Device Analyzer/Curve Tracer for Circuit Design. Available online: https://www.keysight.com/dk/en/product/B1506A/power-device-analyzer-curve-tracer-circuit-design.html (accessed on 17 September 2024).
25. Barón, K.M.; Weiser, M.C.J.; Sharma, K.; Kallfass, I. Analysis of a Transistor-Based On-State Voltage Measurement Circuit for Condition Monitoring of Power Transistors. In Proceedings of the 2023 IEEE Applied Power Electronics Conference and Exposition (APEC), Orlando, FL, USA, 19–23 March 2023; pp. 2556–2562.
26. Gelagaev, R.; Jacqmaer, P.; Driesen, J. A Fast Voltage Clamp Circuit for the Accurate Measurement of the Dynamic ON-Resistance of Power Transistors. *IEEE Trans. Ind. Electron.* **2015**, *62*, 1241–1250. [CrossRef]
27. Weiser, M.C.J.; Barón, K.M.; Fink, T.; Kallfass, I. A Fast ON-State Drain-to-Source Voltage Amplifier for the Dynamic Characterization of GaN Power Transistors. In Proceedings of the 2023 IEEE Applied Power Electronics Conference and Exposition (APEC), Orlando, FL, USA, 19–23 March 2023; pp. 637–644.
28. Rossetto, L.; Spiazzi, G. A Fast ON-State Voltage Measurement Circuit for Power Devices Characterization. *IEEE Trans. Power Electron.* **2022**, *37*, 4926–4930. [CrossRef]
29. Guacci, M.; Bortis, D.; Kolar, J.W. On-state voltage measurement of fast switching power semiconductors. *CPSS Trans. Power Electron. Appl.* **2018**, *3*, 163–176. [CrossRef]